



Internally-externally defects-tailored MAPbI₃ perovskites with highly enhanced air stability and quantum yield

Fengjun Chun, Binbin Zhang, Yuchen Li, Wen Li, Meilin Xie, Xiaodong Peng, Cheng Yan, Zi Chen, Haitao Zhang, Weiqing Yang*

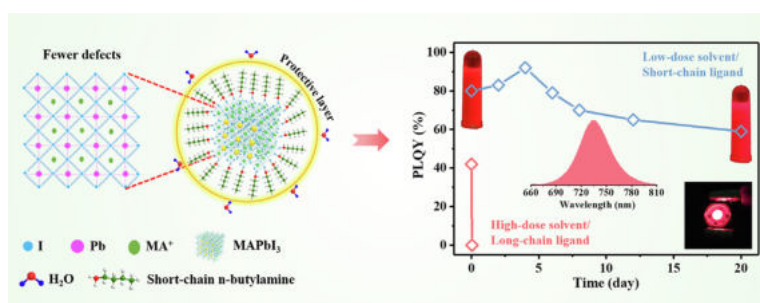
Key Laboratory of Advanced Technologies of Materials (Ministry of Education), School of Materials Science and Engineering, State Key Laboratory of Traction Power, Southwest Jiaotong University, Chengdu 610031, PR China



HIGHLIGHTS

- Air-stable MAPbI₃ was fabricated by solvent dose control and ligand regulation.
- The MAPbI₃ quantum dots exhibit high photoluminescence quantum yield up to 80%.
- The quantum yield was still at 74% of its original value after 20 days.
- The strategy is also suitable for preparing color-tunable MAPbX₃ (X = Cl, Br, I).

GRAPHICAL ABSTRACT



ARTICLE INFO

Keywords:
MAPbI₃ QDs
Perovskite
Low-dose solvent
Short-chain ligand
Improved air stability

ABSTRACT

Methyl-ammonium lead iodide (MAPbI₃) perovskite quantum dots (QDs) have emerged as a promising material for photoelectronic, however, they usually suffer intrinsically from the environmental instability and low photoluminescence quantum yield (PLQY), which will seriously impede their commercial applications. Here, we report an internal-external combination strategy by lowering the dose of good solvent and reducing the chain length of amine ligand to simultaneously enhance the air stability and PLQY of MAPbI₃ QDs. The low-dose solvent can effectively reduce internal iodine vacancies defects and external residual solvent molecules, meanwhile, the faster and denser assembly of nimble short-chain (SC) ligand on the MAPbI₃ QDs surface can helpfully enhance the external surface passivation. As a result, compared to MAPbI₃ QDs synthesized by traditional ligand-assisted reprecipitation (LARP) method, the air stability and PLQY of which are improved by more than four orders of magnitude (from a few minutes to dozens of days) and nearly two times (from 42% to 80%) prepared by our strategy. Besides, this strategy can widely tune the color of MAPbX₃ (X = Cl, Br, I) QDs from 388 to 735 nm through regulating components. This internal-external combination strategy can provide some beneficial enlightenment for preparing long-term air-stable hybrid perovskite QDs with high PLQY, which drastically driving their commercial applications.

1. Introduction

Recently, organic-inorganic hybrid perovskites MAPbX₃ (X = Cl, Br,

I) have caught growing attention due to their marvelous photoelectronic properties, such as large absorption coefficients, small exciton binding energy, high carrier mobility, tunable direct optical bandgap,

* Corresponding author.

E-mail address: wqyang@swjtu.edu.cn (W. Yang).

<https://doi.org/10.1016/j.cej.2020.125715>

Received 19 February 2020; Received in revised form 28 May 2020; Accepted 29 May 2020

Available online 02 June 2020

1385-8947/ © 2020 Elsevier B.V. All rights reserved.

as well as low-cost room temperature processing [1–8]. Nevertheless, due to the weak hydrogen and ionic bonds between inorganic PbX_2 frameworks and organic MA^+ cations, the MAPbX_3 quantum dots (QDs) have an uncanny predisposition toward frequent and rapid degradation in the ambient air [9,10]. Especially for MAPbI_3 QDs, the resulting intrinsically structural instability would easily induce the moisture intrusion into MAPbI_3 QDs and further leading to the formation of colorless intermediate hydrated phases ($\text{MAPbI}_3 \cdot \text{H}_2\text{O}$). This kind of hydrated phase will eventually decompose into PbI_2 and MAI [7–12]. For these reasons, the MAPbI_3 QDs must be encapsulated in the expensive glove box, remarkably forcing up the manufacturing difficulty and cost of the MAPbI_3 QDs based photoelectric devices.

To alleviate the degradation, external capping ligands such as hydrophobic oleic acid (OA), oleylamine (OAm) with long-chain (LC) characteristics have been frequently employed to prepare relatively stable MAPbX_3 QDs by surface passivation strategy [13–18]. Assembly of appropriately capping ligands on the crystal surface not only sufficiently passivate surface defects sites and dangling bonds but also efficiently suppress the interactions between surface atoms and moisture. However, despite all this, such a surface passivation strategy encounters a remarkable challenge to improve the stability of red-emitting MAPbI_3 QDs to date. The LC ligand-passivated MAPbI_3 QDs will completely degrade within a few minutes in the ambient air, and even in a glove box, they will degrade in several weeks or even a few days [19–22]. Such rapid degradation should be ascribed to the fact that these LC ligands are completely helpless for the internal defects despite its effectively repairing partial external defects of MAPbI_3 QDs by surface passivation. In the preparation process, the coordinated polar solvent N, N-Dimethylformamide (DMF) was usually employed as a good solvent for dissolving the inorganic salts and small molecules [23–25]. However, it has a strong binding effect with PbI_2 , which will cause the generation of internal intrinsic crystal defects and further accelerate the degradation of MAPbI_3 QDs [11]. Obviously, it is extremely imminent to explore an effective strategy to simultaneously reduce internal and external defects for the stability improvement of MAPbI_3 QDs.

In this work, we effectively boosted the air stability and photoluminescence quantum yield (PLQY) of the MAPbI_3 QDs by reducing the dose of solvent to lower the internal defects and using nimble short-chain (SC) n-butylamine as capping amine ligand to repair the external defects simultaneously. As a result, the MAPbI_3 QDs can be prepared directly in the ambient air, and the obtained QDs can be exposed to the ambient air for a long time. In detail, the SC n-butylamine-passivated MAPbI_3 QDs prepared with low-dose (1 mL) DMF showed enduring air stability and the PLQY was still at 74% of its original value after 20 days, while the LC n-octylamine-passivated MAPbI_3 QDs prepared with high-dose (4 mL) DMF completely degraded within a few minutes. The far-red-emitting (735 nm) MAPbI_3 QDs with high air stability were coated on an InGaN chip (365 nm) to fabricate a facile light emitting diode (LED) device. This far-red LED can be regarded as an efficient artificial light source for promoting plant growth [26,27]. Moreover, this strategy is also suitable for preparing a collection of color-tunable colloidal MAPbX_3 ($X = \text{Cl}, \text{Br}, \text{I}$) QDs. The corresponding emission spectra can be skillfully regulated from 388 to 735 nm, and the full width at half maximum (FWHM) of the emission spectra is narrow (FWHM = 16 ~ 50 nm). Therefore, we insist that this work could provide worthwhile inspirations and references for improving the stability of organoinorganic hybrid perovskite QDs.

2. Experimental section

2.1. Materials

Methylamine (CH_3NH_2 , 30% in methanol), hydroiodic acid (57% in water), hydrobromic acid (48% in water, 99.99%), lead chloride (PbCl_2 , 99.99%), lead bromide (PbBr_2 , 99%), lead iodide (PbI_2 , 98%), N, N-Dimethylformamide (DMF, 99.5%), n-octylamine (99.5%), n-

butylamine (99.5%) and oleic acid (OA, AR), were purchased from Aladdin. Hydrochloric acid (AR), toluene (AR), and diethyl ether (AR) were purchased from Keshi. All the raw materials were used without further purification.

2.2. Preparation of MAX ($X = \text{Cl}, \text{Br}, \text{I}$)

MAX was prepared by the reported method [13]. First, CH_3NH_2 was dissolved in absolute ethanol, and then HX was slowly added to the solution and constantly mixed in an ice bath. Next, the $\text{CH}_3\text{NH}_2\text{X}$ (MAX) powders were obtained by rotary evaporation. The powder was washed several times with diethyl ether, recrystallized from ethanol, and finally dried in a vacuum oven at 60 °C.

2.3. Preparation of MAPbX_3 ($X = \text{Cl}, \text{Br}, \text{I}$) QDs

MAPbX_3 QDs were prepared using the LARP method. 0.1 mmol MAI and 0.1 mmol PbI_2 were dissolved in 4 mL, 3 mL, 2 mL, 1 mL, 0.5 mL and 0.25 mL DMF, respectively. The precursor solution can be obtained after adding 200 μL OA and 10 μL amine ligand (n-octylamine, hexylamine, n-butylamine, and propylamine) then stirring for 30 min. Then 10 μL precursor solution was added into 4 mL toluene and stirred mightily. Finally, the MAPbI_3 QDs powder was collected by centrifuging for further characterizations. In the same way, a series of color-tunable MAPbX_3 ($X = \text{Cl}, \text{Br}, \text{I}$) QDs were obtained by adjusting the molar ratio of the halogens.

2.4. Fabrication of the far-red LED device

The far-red LED was fabricated by the combination of collected MAPbI_3 QDs powder and UV LED chip. First, a certain amount of red MAPbI_3 QDs phosphors were evenly dispersed in the A glue of silicone. Then, the B glue of silicone was added into the mixture and constantly stirring, and the mass ratio of A glue and B glue of silicone is 1:2. After mixing evenly, the air bubbles of the mixture were evacuated by a vacuum device. Subsequently, the obtained mixture was coated on the surface of the NUV LED chip (365 nm). Last, the red LED device was obtained after drying at 60 °C for 4 h.

2.5. Characterizations

Photoluminescence (PL) spectra of the as-prepared MAPbX_3 ($X = \text{Cl}, \text{Br}, \text{I}$) QDs were collected using FLS980 (Edinburgh Instruments) spectrometer with a 450 W Xenon lamp at room temperature. The time-resolved photoluminescence (TRPL) spectra were recorded by using a 405 nm pulse laser as an excitation source (FLS980). The PLQYs were measured using the fluorescence spectrometer with an integrated sphere (FLS980). The X'Pert Pro (Holland) X-ray diffract meter with $\text{Cu K}\alpha_1$ radiation ($\lambda = 0.154 \text{ nm}$) was exploited to characterize the crystal structures of as-prepared samples. The UV-vis absorption spectra were recorded by the UV-6100 spectrophotometer. The transmission electron microscopy (TEM) and high-resolution transmission electron microscopy (HRTEM) images were measured by a JEP JEM 2100 F field emission transmission electron microscope operating at 200 kV. Thermogravimetric analysis data (TGA) were collected using TGA 5500 (TA Instruments) and heated from 30 to 600 °C at a constant rate of 10 °C min^{-1} under N_2 atmosphere.

3. Result and discussion

To reveal the effect of the good solvent (DMF) dosage on the air stability of MAPbI_3 QDs, a set of LC n-octylamine-passivated MAPbI_3 QDs with various doses of DMF were prepared using the LARP method. The air stability and temporal evolution of PL spectra of these MAPbI_3 QDs were illustrated in Fig. 1 and S1. As shown in Fig. 1a, the emission

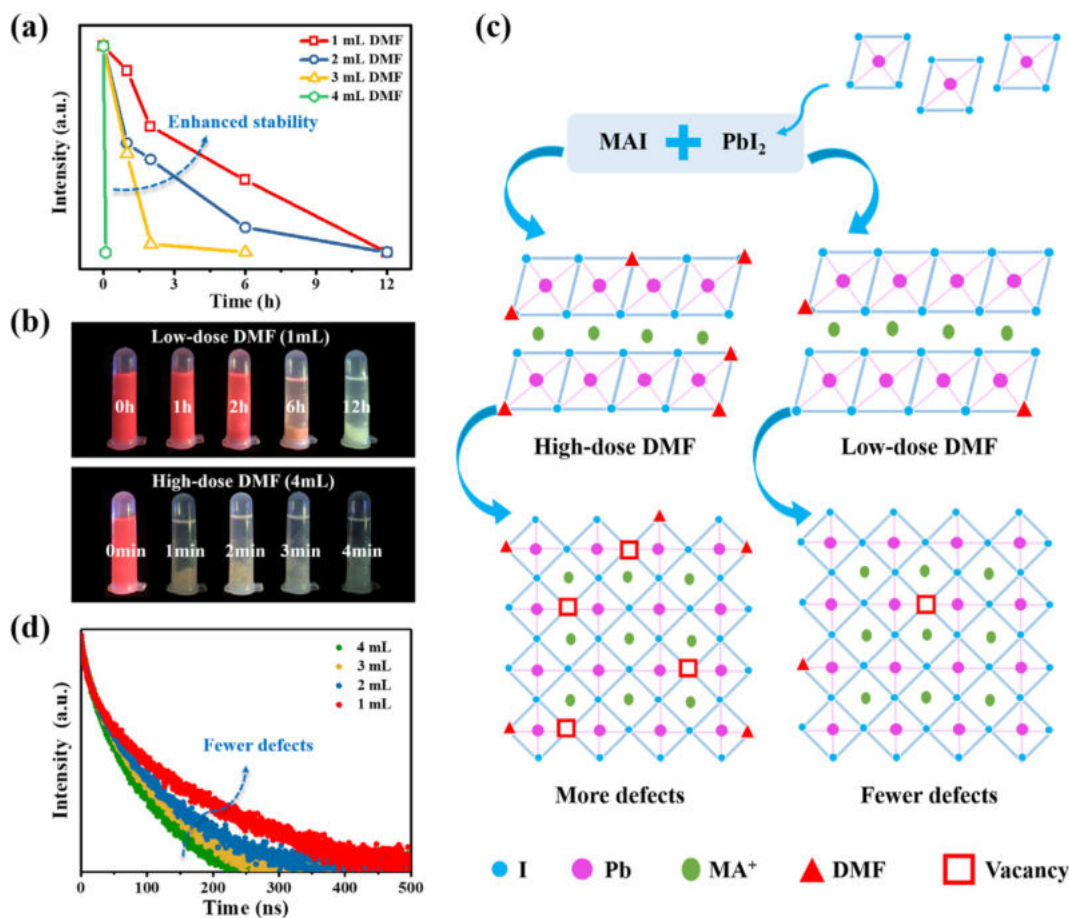


Fig. 1. The effect of various DMF doses on the air stability of LC n-octylamine-passivated MAPbI₃ QDs. (a) Variation of emission intensity with storage time of the MAPbI₃ QDs with different doses of DMF ranging from 1 to 4 mL. (b) Photographs of the MAPbI₃ QDs as a function of the storage time. (c) Schematic illustrations of the transformation process from precursor to MAPbI₃ QDs. (d) TRPL spectra of the MAPbI₃ QDs with various doses of DMF.

intensities of MAPbI₃ QDs show a slower pace of decline with the decrease of DMF dose ranging from 4 mL to 1 mL, obviously indicating that lower-dose DMF will significantly enhance the air stability of the MAPbI₃ QDs. The MAPbI₃ QDs with 4 mL DMF rapidly degraded within a few minutes, while the MAPbI₃ QDs with 1 mL DMF could hold on for more than 6 h, as clearly indicated in Fig. 1b. Such considerably improved air stability of MAPbI₃ QDs with low-dose DMF can be clearly and vividly elucidated by a conceptual model, as schematically illustrated in Fig. 1c. Initially, DMF is employed as a good solvent to completely dissolve MAI, PbI₂ and ligands, MA⁺, Pb²⁺ and I⁻ simultaneously exist as the ionic state in the precursor solution. Next, the precursor solution is quickly added into the anti-solvent (toluene) for the nucleation and growth of MAPbI₃ QDs. However, due to the strong bonding force of DMF and PbI₂, some solvent molecules (DMF) will firmly attach to the surface of MAPbI₃, while some internal iodine vacancies will generate during the removal process of good solvent. These existing internal-external defects will greatly accelerate the degradation of MAPbI₃ QDs, and the number of defects is positively correlated with the dose of DMF. Therefore, reducing the dose of DMF can effectively reduce the number of internal-external defects. Moreover, the LARP method is designed based on supersaturated recrystallization. The supersaturated ions will be precipitated as crystal after transferring the precursor to an insoluble solvent (toluene) [28]. Reducing the dose of good solvent results in a higher degree of supersaturation and induces faster recrystallization of perovskites. This faster recrystallization is contributed to reduce the grain size and hamper aggregation of MAPbI₃. Therefore, appropriately reducing the dose of DMF is a simple and efficient strategy to improve the air stability of MAPbI₃ QDs.

To further confirm the above-proposed model, the TRPL spectra of MAPbI₃ QDs prepared with different doses of DMF were measured to get insight into the defects of MAPbI₃ as well as its exciton recombination dynamics, as shown in Fig. 1d. These decay curves can be fitted well using the bi-exponential function, and the fitting results were summarized in Table S1. The fast lifetimes (τ_1) are related to defect-assisted recombination, and the slow lifetimes (τ_2) are related to radiative recombination [29–31]. With the dose of DMF decreases from 4 mL to 1 mL, the fraction of fast lifetime decreased from 17.70% to 13.89%, revealing the decreased non-radiative recombination. The average lifetimes (τ_{ave}) increase monotonically with the decrease of DMF dosage (the τ_{ave} of MAPbI₃ QDs with 4 mL, 3 mL, 2 mL, and 1 mL are 40.71 ns, 48.06 ns, 55.87 ns, and 77.58 ns, respectively). This monotonic increase of τ_{ave} can evidently confirm that the lower dose of DMF, the fewer defects of MAPbI₃ QDs.

Although the lower dose of DMF can effectively reduce the internal defects of MAPbI₃, it is powerless to repair the external defects, which is also critical essential to improve the air stability of MAPbI₃ QDs. In this work, three other ligands with shorter chain length (n-propylamine, n-butylamine, and n-hexylamine) were employed to passivate the surface defects of MAPbI₃ QDs. The PL spectra and air stability of these three ligands-passivated MAPbI₃ QDs with low-dose (1 mL) DMF were systematically investigated, as shown in Figs. S2 and S3. As the length of amine ligands decreases, the gradual blue shift in the emission spectra can be observed in Fig. S2. The MAPbI₃ QDs passivated by shorter ligands (n-propylamine and n-butylamine) exhibit better air stability than n-hexylamine. The blue-shift emission spectra and increased air stability of MAPbI₃ QDs passivated by shorter ligands may be caused by

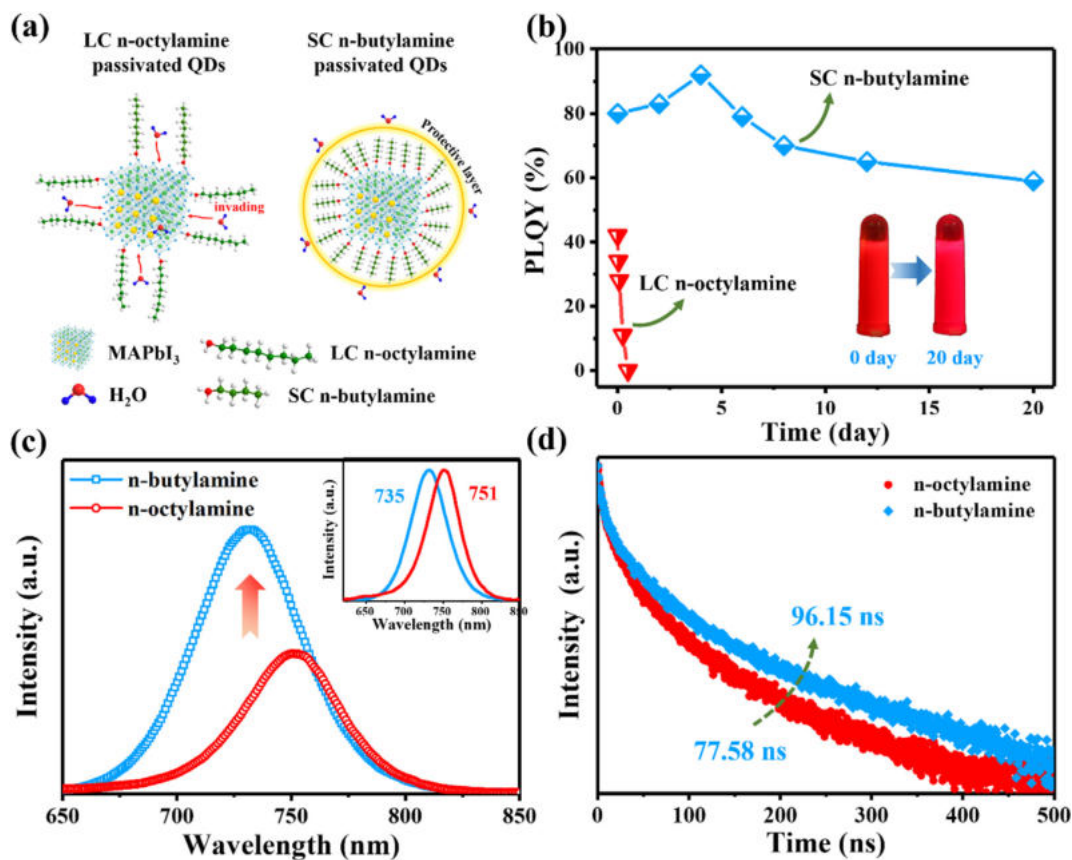


Fig. 2. Comparison of PL properties of LC n-octylamine-passivated MAPbI₃ QDs and SC n-butylamine-passivated MAPbI₃ QDs. (a) The structural model of MAPbI₃ QDs passivated with LC n-octylamine or SC n-butylamine. (b) PLQYs of MAPbI₃ QDs as a function of storage times. (c) PL spectra and (d) TRPL spectra of MAPbI₃ QDs passivated with LC n-octylamine or SC n-butylamine.

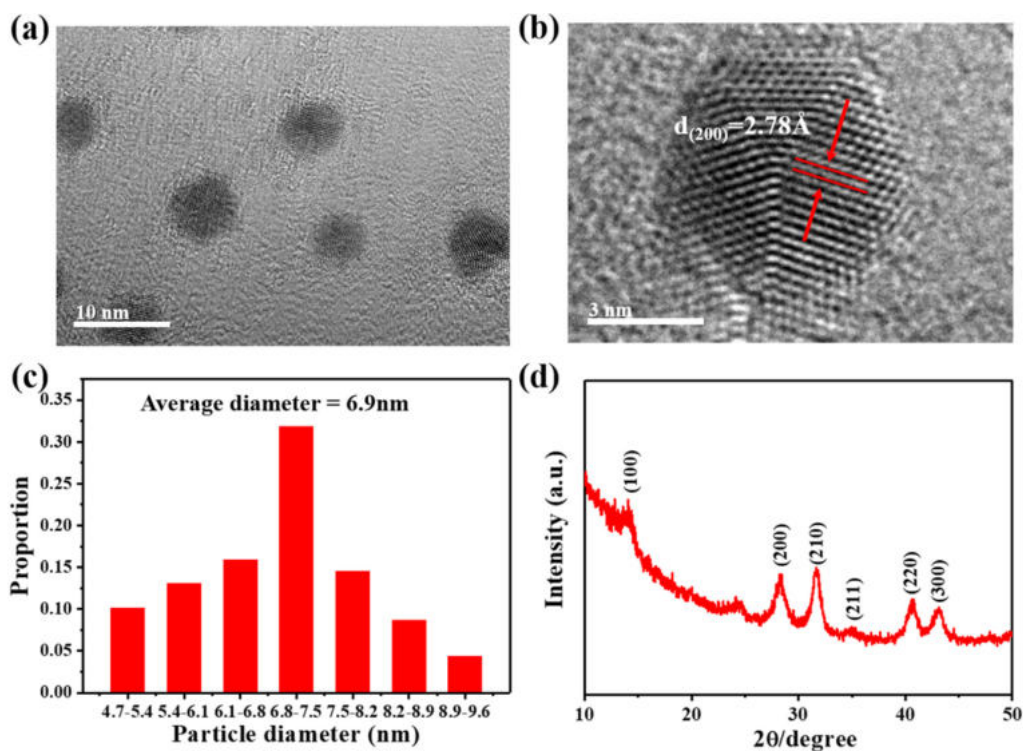


Fig. 3. Morphology and crystal structure of SC n-butylamine-passivated MAPbI₃ QDs with low-dose DMF. (a) TEM image of the MAPbI₃ QDs. (b) HRTEM image of the MAPbI₃ QDs. (c) The corresponding particle size distribution of the MAPbI₃ QDs. (d) The powder XRD pattern of the MAPbI₃ QDs.

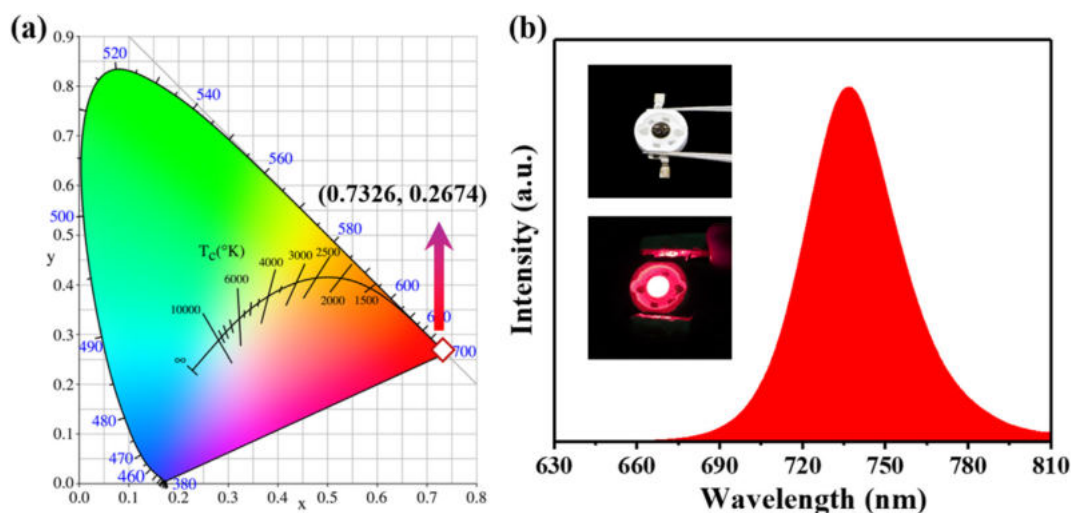


Fig. 4. CIE chromaticity coordinates (a) and the electroluminescence (EL) spectrum (b) of the lighted LED. Inset: the photographs of the fabricated LED.

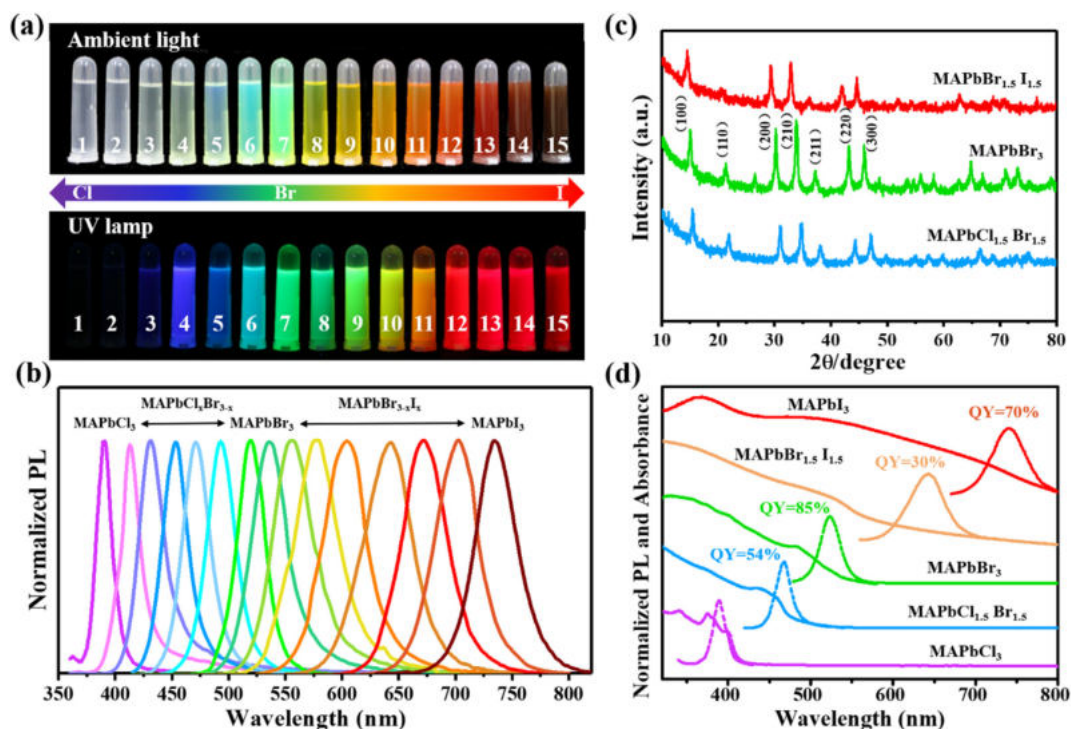


Fig. 5. Steady-state PL properties and crystal structure of SC n-butylamine-passivated MAPbX_3 ($X = \text{Cl}, \text{Br}, \text{I}$) QDs with low-dose DMF. (a) The optical photographs of MAPbX_3 QDs in toluene (Nos. 1–15) under ambient light and UV lamp. (b) The normalized emission spectra of MAPbX_3 ($X = \text{Cl}, \text{Br}, \text{I}$) QDs. (c) XRD patterns of MAPbX_3 ($X = \text{Cl}, \text{Br}, \text{I}$) QDs. (d) The emission and UV-vis absorption spectra of MAPbX_3 ($X = \text{Cl}, \text{Br}, \text{I}$) QDs.

the following two reasons. On the one hand, the shorter amine ligands can faster and compacter assemble on the surface of MAPbI_3 QDs due to the smaller steric hindrance. On the other hand, the shorter amine ligands shows higher polarity compared with the longer ligands, which means the stronger adsorption energy between short-chain n-butylamine and perovskite [32]. However, there is a large redshift (13 nm) of ultra-short n-propylamine-passivated MAPbI_3 QDs after 12 days (Fig. S3g), it is because the agglomeration between adjacent particles cannot be effectively hindered.

To further understand the effect of ligands length on the stability of MAPbI_3 QDs prepared with 1 mL DMF, the comparison analysis method was employed, as shown in Fig. 2. The PLQY of SC n-butylamine-passivated MAPbI_3 QDs and LC n-octylamine-passivated MAPbI_3 QDs are 80% and 42%, respectively. It can be drawn that the luminescent

performance of MAPbI_3 QDs can be effectively improved using SC n-butylamine as passivation ligand. The PLQY of as-prepared MAPbI_3 QDs compares favorably with other reported works, as shown in Fig. S4. Fig. 2b shows the temporal variations of the PLQY of MAPbI_3 passivated with SC n-butylamine or LC n-octylamine, it can be intuitively observed that SC n-butylamine-passivated MAPbI_3 QDs exhibit better stability in ambient air. The LC n-octylamine-passivated MAPbI_3 QDs fully degenerated within 12 h, while the PLQY of SC n-butylamine-passivated MAPbI_3 QDs decreased from 80% to 59% after 20 days. Moreover, there is an obvious enhancement of SC n-butylamine-passivated MAPbI_3 QDs at the beginning of the five days, which can be attributed to the “photobrightening” [33–35]. The formation of lead-oxygen bonds on the surface can be considered as an efficient post-treatment when the MAPbI_3 QDs were exposed to ambient air [33]. The notably improved

air stability of SC n-butylamine-passivated MAPbI₃ QDs can be explained from the following aspects. First, SC n-butylamine is nimbler than the LC n-octylamine under the same experimental conditions, which leads to the rapid assembly of SC n-butylamine ligands on the surface of MAPbI₃ QDs. Such rapid assembly is beneficial to shorten the exposure time of MAPbI₃ QDs. Second, due to the small steric hindrance effect [36,37], SC n-butylamine can more compactly assemble on the MAPbI₃ QDs surface, as shown in Fig. 2a. This compact assembly can better passivate the surface defects of MAPbI₃ QDs. Third, the compact assembly can be considered as a dense hydrophobic protective layer to resist the external moisture intrusion. Last but not least, the stronger adsorption energy between short-chain n-butylamine and perovskite, which could enhance the stability of ligand assembly on MAPbI₃ QDs surface [32]. The compact assembly of n-butylamine on the surface of MAPbI₃ QDs can be confirmed by thermogravimetric analysis (TGA), as shown in Fig. S5. The first major weight loss is caused by the release of CH₃NH₃I and ligands, and the second major weight loss is attributed to the PbI₂ [38]. As we know, the weight percentage of MAI in MAPbI₃ is 25.6%. Based on the TGA data, the weight percentages of MAI, ligands and PbI₂ can be calculated, as shown in Table S2. The higher weight percentage of ligands reveals that n-butylamine is more densely assembled on the surface of MAPbI₃ QDs. On the contrary, the LC n-octylamine and OA are more prone to entanglement, which severely hinders the compact assembly of ligands on the surface of MAPbI₃ QDs. Due to this incompact assembly, some exposed surfaces of MAPbI₃ QDs make moisture intrusion easier. Therefore, the SC n-butylamine-passivated MAPbI₃ QDs exhibit higher air stability than LC n-octylamine-passivated MAPbI₃ QDs. Besides, compared with the insulated LC n-octylamine, the SC n-butylamine is more conducive to the injection and transport of charge in the electroluminescence (EL) device [2,39], as shown in Fig. S6.

The PL spectra of MAPbI₃ QDs passivated with SC n-butylamine and LC n-octylamine are comparatively illustrated in Fig. 2c. It is clearly seen that the emission intensities increase as the length of ligands decreases. MAPbCl₃ and MAPbBr₃ QDs passivated with n-butylamine and n-octylamine have a similar change trend, as shown in Fig. S7. Higher emission intensity appears in the spectra of SC n-butylamine-passivated MAPbX₃ QDs can be ascribed to the enhanced surface passivation. Among the normalized emission spectra of MAPbX₃ QDs in these inserted figures (Fig. 2c, S7c and S7d), SC n-butylamine-passivated MAPbX₃ QDs possess the narrower emission spectra. The narrow emission spectra are originated from the rapid and compact assembly of nimble SC n-butylamine on the surface of perovskites. Such compact coverage can effectively suppress the crystal growth and ensure the uniform size distribution of MAPbX₃ QDs (Fig. S7b). In contrast, the heavy steric hindrance effect and mutual entanglement of LC n-octylamine will increase the difficulty of complete surface passivation, resulting in the uneven size distribution and broadening emission spectra of MAPbX₃ QDs, as shown in Fig. S7a.

The TRPL of MAPbI₃ QDs passivated with SC n-butylamine and LC n-octylamine are shown in Fig. 2d. The decay curves can be well fitted by the biexponential function, the corresponding values are summarized in Table S3. The average lifetimes of MAPbI₃ QDs passivated by LC n-octylamine and SC n-butylamine are calculated to be 77.58 and 96.15 ns, respectively. LC n-octylamine-passivated MAPbI₃ QDs had $\tau_1 = 10.40$ ns ($f_1 = 13.89\%$) and $\tau_2 = 88.42$ ns ($f_2 = 86.11\%$), while SC n-butylamine-passivated MAPbI₃ QDs had $\tau_1 = 10.10$ ns ($f_1 = 9.98\%$) and $\tau_2 = 105.69$ ns ($f_2 = 90.02\%$). The decreased f_1 of SC n-butylamine-passivated MAPbI₃ QDs means that the fraction of defect-assisted recombination lifetime is decreased, which indicates that SC n-butylamine-passivated MAPbI₃ QDs have a fewer surface defect. The increased f_2 of SC n-butylamine-passivated MAPbI₃ QDs reveals the increase of radiative recombination rate, which is very consistent with the increased PLQY [40,41]. Consequently, the combination of low-dose DMF and SC n-butylamine is an effective strategy to enhance the PLQY and air stability of MAPbI₃ QDs. However, the extremely low

dose of DMF is also detrimental to the air stability of MAPbI₃ QDs, as shown in Figs. S8 and S9. Reducing the dose of DMF will increase the supersaturation of the precursor and thus speed up the reaction (nucleation and growth). It is difficult to guarantee the uniformity of size if the reaction speed is too fast, and some unwanted crystal structures and impurities will be generated [28].

The microstructure, size distribution and crystalline structure of MAPbI₃ QDs was investigated by the TEM and XRD, as shown in Fig. 3, S10 and S11. TEM images of SC n-butylamine-passivated MAPbI₃ QDs evidently present the excellent dispersibility with a size distribution ranging from 4 to 10 nm (Fig. 3a) and the average size of about 6.9 nm (Fig. 3c). As shown in Fig. 3b, the lattice plane spacing of 2.34 Å measured in HRTEM corresponds to (2 0 0) plane of cubic phase of MAPbI₃, and the clear lattice fringes reveal that the high crystallinity of MAPbI₃ QDs. Fig. 3d obviously presents that the XRD pattern of the sample can be matched well with the cubic-phase CH₃NH₃PbI₃ [42–44]. The typical diffraction peaks at 2θ with 14.06°, 28.42°, 31.66°, 34.98°, 40.76° and 43.16° correspondingly are (1 0 0), (2 0 0), (2 1 0), (2 1 1), (2 2 0) and (3 0 0), respectively. These results suggest that SC n-butylamine can be a common and excellent ligand for preparing MAPbI₃ QDs.

In order to further determine the potential utilization value of MAPbI₃ QDs in plant cultivation LEDs, a far-red-emitting LED was fabricated using a combination of UV chip and as-prepared sample. The EL spectrum of the fabricated LED is shown in Fig. 4b, the far-red emission light (735 nm) can be exploited to accelerate the growth of the indoor plants [26,27]. The CIE chromaticity coordinated of the fabricated LED is (0.7326, 0.2674), and the coordinate position is labeled as a diamond in the CIE chromaticity diagram, as shown in Fig. 4a.

Furthermore, this combination strategy can be also extended to synthesize an array of spectrum-tunable MAPbX₃ QDs from near-ultraviolet (NUV) to visible region by accurately controlling the composition ratio of halogen. Fig. 5a and 5b present the color-tunable photographs of a range of MAPbX₃ (X = Cl, Br, I) QDs under ambient and UV light as well as their normalized emission spectra (further information is summarized in Table S4). The emission wavelength of MAPbX₃ can be adjusted from 388 to 735 nm, and the FWHM of the emission spectra are ranging from 16 to 50 nm. Compared with previous reports, the blue-shifted emission wavelength of MAPbCl₃ may be ascribed to the quantum size effect. The rapid and compact assembly of nimble SC n-butylamine can effectively inhibit the growth and aggregation of MAPbCl₃ QDs. The XRD patterns of SC n-butylamine-passivated MAPbX₃ QDs with various compositions are illustrated in Fig. 5c. All these samples present a similar cubic structure of MAPbBr₃ [11], obviously revealing hardly changed crystal structure with changing composition. Fig. 5d presents the PL emission spectra and UV–vis absorption spectra of MAPbX₃. For MAPbBr₃, there is a strong absorption peak at 480 nm and its Stokes shift (SS) is calculated to be about 40 nm. This large SS can effectively improve the PLQY (85%) of MAPbBr₃ due to the low self-absorption [45,46]. The corresponding PLQYs of as-prepared MAPbX₃ are listed in Fig. 5d. Furthermore, the TEM images, HRTEM images and size distribution of n-butylamine-passivated MAPbCl₃ and MAPbBr₃ QDs are shown in Fig. S12. The average particle sizes of MAPbCl₃ and MAPbBr₃ QDs were 4.3 nm and 4.7 nm, respectively. These results evidently indicate the excellent effectiveness of this internal-external combination strategy for the preparation of MAPbX₃ QDs with high air stability, adjustable emission spectra, high PLQY, and high crystallization.

4. Conclusion

In this paper, we have reported an ingenious and simple combination strategy to prepare air-stable MAPbI₃ QDs by simultaneously reducing internal-external defects. Reducing the dose of DMF is one of the simplest but most powerful ways to reduce the internal iodine vacancies and external residual solvent molecules, thereby achieving the

objective of reducing internal crystal defects. Meanwhile, using nimble SC n-butylamine as amine ligand can effectively repair the external surface defects of MAPbX₃ QDs, and the formed compact hydrophobic protective layer can effectively resist the invasion of moisture. This faultless combination between reduced defect and enhanced surface passivation can significantly improve the stability of MAPbI₃ QDs in ambient air. The PLQY of SC n-butylamine-passivated MAPbI₃ with low-dose DMF still maintained 59% after 20 days, while LC n-octylamine-passivated MAPbX₃ QDs with high-dose DMF rapidly degraded in only a few minutes. Moreover, due to the enhanced surface passivation, the PLQY of SC n-butylamine-passivated MAPbI₃ QDs (80%) is much higher than LC n-octylamine-passivated MAPbI₃ QDs (42%). These high-efficiency red MAPbI₃ QDs with long-term air-stability have considerable application foreground in plant cultivation LEDs. Except for these, this combination strategy could be extended to prepare a series of color-tunable (388 ~ 735 nm) MAPbX₃ QDs with narrow FWHM and high PLQY. Evidently, these results provide some new inspiration for further realizing the high stability, high efficiency and commercial application of MAPbX₃ QDs.

Declaration of Competing Interest

The authors declare that they have no known competing financial interests or personal relationships that could have appeared to influence the work reported in this paper.

Acknowledgments

This work is supported by the National Natural Science Foundation of China (No.61801403), the Scientific and Technological projects for International Cooperation Funds of Sichuan Province (No. 2017HH0069), the Fundamental Research Funds for the Central Universities of China (A0920502051619-72), Doctoral Innovation Fund Program of Southwest Jiaotong University. The authors also gratefully acknowledge ceshigo (www.ceshigo.com) for providing testing services.

References

- N.J. Jeon, J.H. Noh, Y.C. Kim, W.S. Yang, S. Ryu, S.I. Seok, Solvent engineering for high-performance inorganic-organic hybrid perovskite solar cells, *Nat. Mater.* 13 (2014) 897–903.
- Y.H. Kim, G.H. Lee, Y.T. Kim, C. Wolf, H.J. Yun, W. Kwon, C.G. Park, T.W. Lee, High efficiency perovskite light-emitting diodes of ligand-engineered colloidal formamidinium lead bromide nanoparticles, *Nano Energy* 38 (2017) 51–58.
- Q. Li, H. Li, H. Shen, F. Wang, F. Zhao, F. Li, X. Zhang, D. Li, X. Jin, W. Sun, Solid ligand-assisted storage of air-stable formamidinium lead halide quantum dots via restraining the highly dynamic surface toward brightly luminescent light-emitting diodes, *ACS Photonics* 4 (2017) 2504–2512.
- C. Liu, Z. Qiu, W. Meng, J. Chen, J. Qi, C. Dong, M. Wang, Effects of interfacial characteristics on photovoltaic performance in CH₃NH₃PbBr₃ - based bulk perovskite solar cells with core/shell nanoarray as electron transporter, *Nano Energy* 12 (2015) 59–68.
- G. Niu, X. Guo, L. Wang, Review of recent progress in chemical stability of perovskite solar cells, *J. Mater. Chem. A* 3 (2015) 8970–8980.
- Y. Shi, P. Duan, S. Huo, Y. Li, M. Liu, Endowing perovskite nanocrystals with circularly polarized luminescence, *Adv. Mater.* 30 (2018) e1705011.
- O. Selig, A. Sadhanala, C. Müller, R. Lovrincic, Z. Chen, Y.L.A. Rezes, J.M. Frost, T.L.C. Jansen, A.A. Bakulin, Organic cation rotation and immobilization in pure and mixed methylammonium lead-halide perovskites, *J. Am. Chem. Soc.* 139 (2017) 4068–4074.
- K. Jung, W.S. Chae, Y.C. Park, J. Kim, M.J. Lee, Influence of Lewis base HMPA on the properties of efficient planar MAPbI₃ solar cells fabricated by one-step process assisted by Lewis acid-base adduct approach, *Chem. Eng. J.* 380 (2020) 122436.
- Q. Wang, B. Chen, Y. Liu, Y. Deng, Y. Bai, Q. Dong, J. Huang, Scaling behavior of moisture-induced grain degradation in polycrystalline hybrid perovskite thin films, *Energy Environ. Sci.* 10 (2017) 516–522.
- Y. Huang, F. Li, L. Qiu, F. Lin, Z. Lai, S. Wang, L. Lin, Y. Zhu, Y. Wang, Y. Jiang, X. Chen, Enhancing the stability of CH₃NH₃PbBr₃ nanoparticles using double hydrophobic shells of SiO₂ and poly(vinylidene fluoride), *ACS Appl. Mater. Interfaces* 11 (2019) 26384–26391.
- F. Zhang, S. Huang, P. Wang, X. Chen, S. Zhao, Y. Dong, H. Zhong, Colloidal synthesis of air-stable CH₃NH₃PbI₃ quantum dots by gaining chemical insight into the solvent effects, *Chem. Mater.* 29 (2017) 3793–3799.
- D. Yang, W. Ming, H. Shi, L. Zhang, M.H. Du, Fast diffusion of native defects and impurities in perovskite solar cell material CH₃NH₃PbI₃, *Chem. Mater.* 28 (2016) 4349–4357.
- F. Zhang, H. Zhong, C. Chen, X. Wu, X. Hu, H. Huang, J. Han, B. Zou, Y. Dong, Tunable colloidal CH₃NH₃PbX₃ (X = Br, I, Cl) quantum dots: potential alternatives for display technology, *ACS Nano* 9 (2015) 4533–4542.
- I. Levchuk, P. Herre, M. Brandl, A. Osvet, R. Hock, W. Peukert, P. Schweizer, E. Spiecker, M. Batentschuk, C.J. Brabec, Ligand-assisted thickness tailoring of highly luminescent colloidal CH₃NH₃PbX₃ (X = Br and I) perovskite nanoplatelets, *Chem. Commun.* 53 (2016) 244–247.
- J. Pan, Y. Shang, J. Yin, M. De Bastiani, W. Peng, I. Dursun, L. Sinatra, A.M. El-Zohry, M.N. Hedhili, A. Emwas, O.F. Mohammed, Z.J. Ning, M.O. Bakr, Bidentate ligand-passivated CsPbI₃ perovskite nanocrystals for stable near-unity photoluminescence quantum yield and efficient red light-emitting diodes, *J. Am. Chem. Soc.* 140 (2018) 562–565.
- B. Li, C. Fei, K. Zheng, X. Qu, T. Pullerits, G. Cao, J. Tian, Constructing water-resistant CH₃NH₃PbI₃ perovskite films via coordination interaction, *J. Mater. Chem. A* 4 (2016) 17018–17024.
- S. Chen, X. Wen, J. Yun, S. Huang, M. Green, N. Jeon, W. Yang, J. Noh, J. Seo, S. Seok, A. Ho-Baillie, Spatial distribution of lead iodide and local passivation on organo-lead halide perovskite, *ACS Appl. Mater. Interfaces* 9 (2017) 6072–6078.
- H. Sun, Z. Yang, M. Wei, W. Sun, X. Li, S. Ye, Y. Zhao, H. Tan, E.L. Kynaston, T.B. Schon, H. Yan, Z. Lu, G.A. Ozin, E.H. Sargent, D.S. Seferos, Chemically addressable perovskite nanocrystals for light-emitting applications, *Adv. Mater.* 29 (2017) 1701153.
- Y. Han, S. Meyer, Y. Dkhissi, K. Weber, J.M. Pringle, U. Bach, L. Spiccia, Y.B. Cheng, Degradation observations of encapsulated planar CH₃NH₃PbI₃ perovskite solar cells at high temperatures and humidity, *J. Mater. Chem. A* 3 (2015) 8139–8147.
- T.P. Gujar, T. Unger, A. Schonleber, M. Fried, F. Panzer, S. van Smaalen, A. Kohler, M. Thelakktat, The role of PbI₂ in CH₃NH₃PbI₃ perovskite stability, solar cell parameters and device degradation, *Phys. Chem. Chem. Phys.* 20 (2017) 605–614.
- G. Divitini, S. Cacovich, F. Matteocci, L. Cinà, A. Di Carlo, C. Ducati, In situ observation of heat-induced degradation of perovskite solar cells, *Nat. Energy* 1 (2016) 15012.
- J. Yang, B.D. Siempelkamp, D. Liu, T.L. Kelly, Investigation of CH₃NH₃PbI₃ degradation rates and mechanisms in controlled humidity environments using in situ techniques, *ACS Nano* 9 (2015) 1955–1963.
- D. Shen, X. Yu, X. Cai, M. Peng, Y. Ma, X. Su, L. Xiao, D. Zou, Understanding the solvent-assisted crystallization mechanism inherent in efficient organic-inorganic halide perovskite solar cells, *J. Mater. Chem. A* 2 (2014) 20454–20461.
- Y. Zhao, K. Zhu, Solution chemistry engineering toward high-efficiency perovskite solar cells, *J. Phys. Chem. Lett.* 23 (2014) 4175–4186.
- W. Zhu, C. Bao, F. Li, T. Yu, H. Gao, Y. Yi, J. Yang, G. Fu, X. Zhou, Z. Zou, A halide exchange engineering for CH₃NH₃PbI_{3-x}Br_x perovskite solar cells with high performance and stability, *Nano Energy* 19 (2016) 17–26.
- Z. Zhang, L. Shen, H. Zhang, L. Ding, G. Shao, X. Liang, W. Xiang, Novel red-emitting CsPb_{1-x}Ti_xI₃ perovskite QDs @ glasses with ambient stability for high efficiency white LEDs and plant growth LEDs, *Chem. Eng. J.* 378 (2019) 122125.
- J. Liang, B. Devakumar, L. Sun, Q. Sun, S. Wang, B. Li, D. Chen, X. Huang, Mn⁴⁺-activated KLaMgWO₆: a new high-efficiency far-red phosphor for indoor plant growth LEDs, *Ceram. Int.* 45 (2019) 4564–4569.
- X. Li, Y. Wu, S. Zhang, B. Cai, Y. Gu, J. Song, H. Zeng, CsPbX₃ quantum dots for lighting and displays: room temperature synthesis, photoluminescence superiorities, underlying origins and white light-emitting diodes, *Adv. Funct. Mater.* 26 (2016) 2435–2445.
- Z. Wang, T. Cheng, F. Wang, S. Dai, Z. Tan, Morphology engineering for high-performance and multicolored perovskite light-emitting diodes with simple device structures, *Small* 12 (2016) 4412–4420.
- Y. Zhao, X. Xu, X. You, Colloidal organometal halide perovskite (MAPbBr_xI_{3-x})_{0 < x ≤ 3} quantum dots: controllable synthesis and tunable photoluminescence, *Sci. Rep.* 6 (2016) 35931.
- K. Hills-Kimball, Y. Nagaoka, C. Cao, E. Chaykovsky, O. Chen, Synthesis of formamidinium lead halide perovskite nanocrystals through solid-liquid-solid cation exchange, *J. Mater. Chem. C* 5 (2017) 5680–5684.
- Y. Yuan, Z. Liu, Z. Liu, L. Peng, Y. Li, A. Tang, Photoluminescence and self-assembly of cesium lead halide perovskite nanocrystals: effects of chain length of organic amines and reaction temperature, *Appl. Surf. Sci.* 405 (2017) 280–288.
- J.S.W. Godding, A.J. Ramadan, Y.H. Lin, K. Schutt, H.J. Snaith, B. Wenger, Oxidative passivation of metal halide perovskites, *Joule* 3 (2019) 2716–2731.
- Y. Wei, Z.Y. Cheng, J. Lin, An overview on enhancing the stability of lead halide perovskite quantum dots and their applications in phosphor-converted LEDs, *Chem. Soc. Rev.* 48 (2019) 310–350.
- H. Hu, L. Wu, Y. Tan, Q. Zhong, M. Chen, Y. Qiu, D. Yang, B. Sun, Q. Zhang, Y. Yin, Interfacial synthesis of highly stable CsPbX₃/oxide janus nanoparticles, *J. Am. Chem. Soc.* 140 (2018) 406–412.
- R. Azmi, S. Sinaaga, H. Aqoma, G. Seo, T.K. Ahn, M. Park, S.Y. Ju, J.W. Lee, T.W. Kim, S.H. Oh, S.Y. Jang, Highly efficient air-stable colloidal quantum dot solar cells by improved surface trap passivation, *Nano Energy* 39 (2017) 86–94.
- K. Chen, Q. Zhong, W. Chen, B. Sang, Y. Wang, T. Yang, Y. Liu, Y. Zhang, H. Zhang, Short-chain ligand-passivated stable α-CsPbI₃ quantum dot for all-inorganic perovskite solar cells, *Adv. Funct. Mater.* 29 (2019) 1900991.
- C. Geng, S. Xu, H. Zhong, A.L. Rogach, W. Bi, Aqueous synthesis of methylammonium lead halide perovskite nanocrystals, *Angew. Chem. Int. Ed.* 57 (2018) 9650–9654.
- J. Dai, J. Xi, L. Li, J. Zhao, Y. Shi, W. Zhang, C. Ran, B. Jiao, X. Hou, X. Duan, Z. Wu,

- Charge transport between coupling colloidal perovskite quantum dots assisted by functional conjugated ligands, *Angew. Chem. Int. Ed.* 57 (2018) 5754–5758.
- [40] C. Luo, W. Li, D. Xiong, J. Fu, W. Yang, Surface pre-optimization of a mixed halide perovskite toward high photoluminescence quantum yield in the blue spectrum range, *Nanoscale* 11 (2019) 15206–15215.
- [41] M. Wang, Q. Fu, L. Yan, J. Huang, Q. Ma, M. Huamayun, W. Pi, X. Chen, Z. Zheng, W. Luo, Systematic optimization of perovskite solar cells via green solvent systems, *Chem. Eng. J.* 387 (2020) 123966.
- [42] H. Wei, D. DeSantis, W. Wei, Y. Deng, D. Guo, T.J. Savenije, L. Cao, J. Huang, Dopant compensation in alloyed $\text{CH}_3\text{NH}_3\text{PbBr}_{3-x}\text{Cl}_x$ perovskite single crystals for gamma-ray spectroscopy, *Nat. Mater.* 16 (2017) 826–833.
- [43] A. Xie, T.H. Nguyen, C. Hettiarachchi, M.E. Witkowski, W. Drozdowski, M.D. Birowosuto, H. Wang, C. Dang, Thermal quenching and dose studies of x-ray luminescence in single crystals of halide perovskites, *J. Phys. Chem. C* 122 (2018) 16265–16273.
- [44] T. Baikie, Y. Fang, J.M. Kadro, M. Schreyer, F. Wei, S.G. Mhaisalkar, M. Graetzel, T.J. White, Synthesis and crystal chemistry of the hybrid perovskite $(\text{CH}_3\text{NH}_3)\text{PbI}_3$ for solid-state sensitised solar cell applications, *J. Mater. Chem. A* 1 (2013) 5628–5641.
- [45] M. Leng, Y. Yang, K. Zeng, Z. Chen, Z. Tan, S. Li, J. Li, B. Xu, D. Li, M.P. Hautzinger, Y. Fu, T. Zhai, L. Xu, G. Niu, S. Jin, J. Tang, All-inorganic bismuth-based perovskite quantum dots with bright blue photoluminescence and excellent stability, *Adv. Funct. Mater.* 28 (2018) 1704446.
- [46] A.M. Smith, S. Nie, Semiconductor nanocrystals: structure, properties, and band gap engineering, *Acc. Chem. Res.* 43 (2010) 190–200.